

Simulation of a two-dimensional sheath over a flat insulator–conductor interface on a radio-frequency biased electrode in a high-density plasma

Doosik Kim and Demetre J. Economou^{a)}

Plasma Processing Laboratory, Department of Chemical Engineering, University of Houston, Houston, Texas 77204-4004

(Received 28 August 2003; accepted 8 January 2004)

A combined fluid/Monte Carlo (MC) simulation was developed to study the two-dimensional (2D) sheath over a flat insulator/conductor interface on a radio-frequency (rf) biased electrode in a high-density plasma. The insulator capacitance increased the local impedance between the plasma and the bias voltage source. Thus, for uniform ion density and electron temperature far away from the wall, the sheath potential over the insulator was only a fraction of that over the conductor, resulting in a thinner sheath over the insulator. The fluid model provided the spatiotemporal profiles of the 2D sheath electric field. These were used as input to the MC simulation to compute the ion energy distribution (IED) and ion angular distribution (IAD) at different locations on the surface. The ion flux, IED, and IAD changed drastically across the insulator/conductor interface due to the diverging rf electric field in the distorted sheath. The ion flux was larger on the conductor at the expense of that on the insulator. Both the ion impact angle and angular spread increased progressively as the material interface was approached. The ion impact energy and energy spread were smaller on the insulator as compared to the conductor. For given plasma parameters, as the insulator thickness was increased, the sheath potential and thickness over the insulator decreased, and sheath distortion became more pronounced. © 2004 American Institute of Physics.

[DOI: 10.1063/1.1652249]

I. INTRODUCTION

A sheath forms over any surface in contact with plasma. The sheath over a flat, infinite, homogeneous surface is one dimensional, with the sheath electric field pointing perpendicular to the surface. When the surface contains topographical features, however, the sheath is no longer one dimensional. The extent of sheath “disturbance” depends on the thickness of the sheath compared to the size of the topographical features. When the sheath thickness is comparable to or smaller than the length scale of the surface features, the sheath tends to wrap around the contour of the features. This is called *plasma molding*. We have reported self-consistent simulations of plasma molding and the resulting energy and angular distributions of ions and energetic neutrals along surface topography: Step,^{1,2} trench,³ and ring.⁴ Experimental measurements of ion energy and angular distributions modified by plasma molding were presented in Ref. 5.

A multidimensional sheath can also arise over a flat surface with material discontinuities, as depicted in Fig. 1. A flat surface with an insulator/conductor interface is exposed to plasma. The backing electrode is biased with a radio-frequency (rf) voltage source. The insulator provides an additional impedance and part of the applied bias voltage is dropped across the insulator. This makes the sheath potential over the insulator smaller than that over the adjacent conductor. Thus, for given uniform plasma parameters (plasma density, electron temperature, i.e., Debye length), the sheath is thicker over the conductor side, compared to that over the

insulator side. A schematic of the plasma–sheath interface (sheath edge) is also shown in Fig. 1. Due to the distorted sheath edge, the sheath electric field is no longer perpendicular to the surface in the vicinity of the insulator/conductor interface. The multidimensional electric field diverts oncoming ions from their otherwise vertical trajectories. The ion flux, ion energy distribution (IED), and ion angular distribution (IAD) across the interface can be drastically different, depending on the extent of sheath distortion.

We have reported simulations of a two-dimensional (2D) sheath and the resulting ion flow over a flat surface with an insulator–conductor interface under the influence of a direct-current (dc) bias.⁶ The insulator attained the floating potential under the dc condition. Owing to the diverging sheath field, the ion impact angle along the surface increased progressively as the material interface was approached, and the ion flux was higher on the conductor side at the expense of that on the insulator side. The spatial extent and magnitude of the ion flux disturbance was found to scale with the difference in the sheath thickness over the two materials. Sheath distortion was more pronounced when the electron temperature decreased, or the dc bias was made more negative, or the secondary electron emission coefficient of the insulator increased.

In the case of rf bias, the insulator presents an additional capacitance (C_d) in series with the sheath capacitance (C_s). The sheath potential over the insulator depends on the ratio C_s/C_d . For a given bias voltage, as C_d decreases compared to C_s , a larger fraction of the applied bias drops across the insulator, and the sheath distortion is exacerbated. Hoekstra and Kushner⁷ observed that a subwafer dielectric ring caused

^{a)}Electronic mail: economou@uh.edu

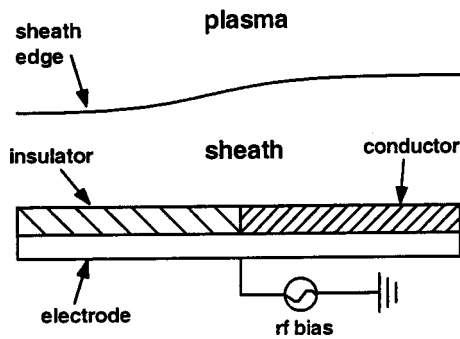


FIG. 1. Schematic (not to scale) of 2D (x,y) sheath formation over a flat inhomogeneous substrate in contact with plasma. Half of the substrate is insulating and the other half is conductive. Both the insulator and the conductor are assumed to be of a semi-infinite extent. The backing electrode is biased using a rf voltage source. The sheath potential and thickness are larger over the conductor, compared to the insulator, resulting in a 2D sheath.

a local reduction in the ion energy and flux on the wafer in their plasma etching reactor simulation.

In this article, we report a combined fluid/Monte Carlo (MC) simulation of a 2D rf sheath over a flat surface with an insulator–conductor interface in contact with a high-density Ar plasma. The self-consistent fluid simulation predicted the spatiotemporal profiles of the sheath electric field. These were used as input to the MC simulation to predict the IED and IAD at different locations along the surface. A similar fluid/MC approach was followed in studies of plasma molding over topographical features reported earlier.^{1–4} This report focuses on the effect of insulator capacitance on sheath distortion, with given uniform plasma parameters. The effect of plasma parameters on sheath distortion for the dc case was discussed in a previous report.⁶

II. SURFACE CHARGING OF AN INSULATOR

Surfaces in contact with plasma receive particle (electrons, ions) currents from the plasma. Although a conductor can remain equipotential,⁸ charge accumulates on an insulator surface until, for a dc case, the floating potential is reached at steady state.^{6,9,10} The floating potential is negative with respect to the plasma, repelling incoming electrons to balance the positive ion and electron currents.

In a rf case, a displacement current also flows through the sheath and the insulator. The surface potential and charge density on the insulator surface depend on the electrical properties of the insulator and the sheath. The situation where a flat insulator of an infinite extent is exposed to plasma is depicted in Fig. 2. The thickness and permittivity of the insulator are d and ϵ , respectively. The bottom of the insulator is biased at $\Phi_b(t)$ while the insulator surface attains potential $\Phi_w(t)$. Due to the existence of surface charge ρ_s , the normal component of the electric field must be discontinuous across the sheath–insulator interface,^{11,12}

$$\rho_s = \epsilon E - \epsilon_0 E_0, \quad (1)$$

where E_0 and E are the normal components of the electric field on the sheath side and the insulator side, respectively, of

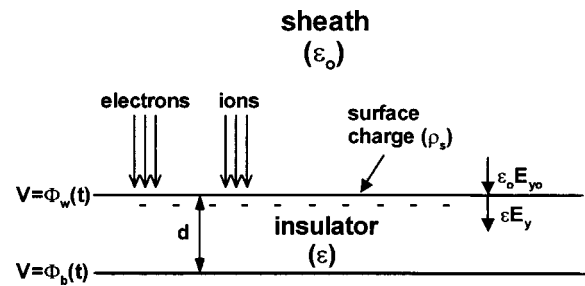


FIG. 2. Surface charging of a rf biased flat insulator of infinite extent exposed to plasma. Ion and electron flow from the plasma result in accumulation of surface charge on the insulator. Surface charge causes the normal component of the electric field to be discontinuous across the interface. The surface potential of the insulator is $\Phi_w(t)$ and the rf bias is $\Phi_b(t)$.

the interface. Since the surface charge is due to particle currents coming from the plasma, the time rate of change of the surface charge density is given by

$$\frac{\partial \rho_s}{\partial t} = eJ_i - eJ_e, \quad (2)$$

where e is the elementary charge and J_i and J_e are the flux of positive ions and electrons, respectively, onto the surface.

An equivalent circuit model of the sheath over the insulator is shown in Fig. 3.^{9,13} The insulator presents a capacitance C_d while the sheath capacitance is C_s . The ion current is represented by a current source, while the nonlinear electron current is shown as a diode. The capacitance of the insulator increases the local impedance between the plasma and the bias voltage source, reducing the sheath potential. As the ratio C_d/C_s decreases (e.g., thicker insulator), the local impedance of the insulator increases leading to a larger potential drop across the insulator.

III. NUMERICAL MODEL AND SIMULATION PROCEDURES

A. Fluid simulation

The fluid model employed in this study predicted the 2D (x,y) rf sheath electric field and the resulting ion flow in a self-consistent manner.^{1–4,6} An electropositive plasma with one type of positive ion and electrons was considered. The

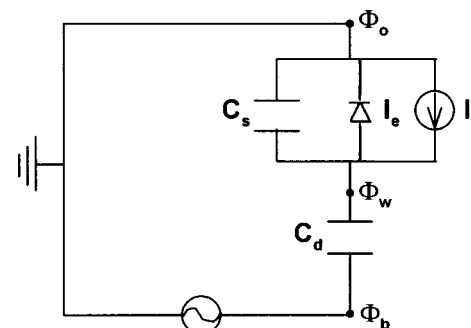


FIG. 3. Equivalent circuit model for the rf biased insulator shown in Fig. 2. The insulator presents a capacitance C_d in series with the sheath capacitance C_s . The ion current is represented by a current source and the nonlinear electron current is modeled as a diode.

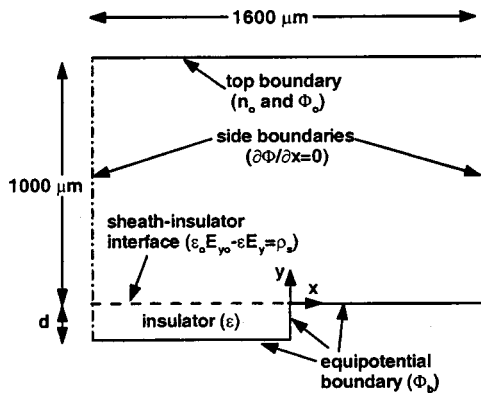


FIG. 4. Simulation domain and boundary conditions. The potential and electron density were specified at the top boundary. The potential on either side of the boundary was assumed to vary only in the vertical direction. The rf bias voltage $\Phi_b(t)$ was specified along the equipotential boundary at the bottom. [Equation (1) was applied at the sheath–insulator interface.]

governing equations were the mass and momentum conservation equations for ions, coupled with Poisson’s equation for the electric potential. The ion distribution function was a drifting Maxwellian, whereas electrons were Maxwellian at temperature T_e . The Boltzmann relation was used for the electron density, neglecting electron inertia. Since electrons see only a repelling potential in the sheath, the electron distribution function should remain Maxwellian at the same temperature.¹⁰ The background neutral gas pressure and temperature (hence, density) were taken to be uniform throughout.

The ion mass and momentum balance equations read

$$\frac{\partial n_i}{\partial t} + \nabla \cdot (n_i \mathbf{u}) = 0, \quad (3)$$

$$\frac{\partial}{\partial t} (n_i \mathbf{u}) + \nabla \cdot (n_i \mathbf{u} \mathbf{u}) = -\frac{en_i}{m_i} \nabla \Phi - \nu_m n_i \mathbf{u}, \quad (4)$$

where n_i , m_i , and \mathbf{u} are the ion density, ion mass, and ion fluid velocity, respectively. Φ is the electric potential and e is the elementary charge. ν_m is the total collision frequency for momentum exchange of ions (elastic scattering and charge exchange collisions) with the background gas. The ion pressure force was ignored because the ion thermal energy is much lower than the drift energy (cold ion approximation). However, thermal effects were accounted for in the MC simulation. Note also that any ionization in the computational domain (Fig. 4) has been ignored [right-hand side of Eq. (3) equal to zero]. This is because of the small size of the computational domain and the large ion current flowing into the domain from the plasma.

Poisson’s equation with the Boltzmann relation for electrons reads

$$\nabla^2 \Phi = -\frac{e}{\epsilon_0} \left(n_i - n_0 \exp\left(\frac{\Phi - \Phi_0}{T_e}\right) \right), \quad (5)$$

where ϵ_0 is the permittivity of free space, T_e is the electron temperature (in V), and Φ_0 and n_0 are the values for electric potential and ion density, respectively, at the top boundary of the domain (see Fig. 4). Equation (5) was solved in the

sheath region. The Laplace equation $\nabla^2 \Phi = 0$ was solved inside the insulator, since the charge is confined at the insulator surface (boundary condition).

The simulation domain and boundary conditions are shown in Fig. 4. The origin $(x,y)=(0,0)$ of the coordinate system is at the insulator–conductor interface. The insulator occupies the space $x < 0$ and $-d < y \leq 0$. The conductor occupies the space $x \geq 0$ and $y \leq 0$. The sheath occupies the space $y > 0$. The ion mass and momentum equations were solved in the sheath space ($0 < y < 1000 \mu\text{m}$). The plasma density (n_0) and plasma potential (Φ_0) were specified at the top boundary and were assumed to be spatially uniform. The top boundary was always thicker than the resulting sheath. In the simulation, the potential of the top surface Φ_0 was set equal to zero (reference value) and the applied bias Φ_b was specified along the conducting boundary ($y = -d$ for $x < 0$, $-d < y \leq 0$ for $x = 0$, and $y = 0$ for $x \geq 0$). The potential was assumed to vary only in the vertical direction on either side boundary, i.e., a one-dimensional sheath away from the insulator–conductor interface. Poisson’s Eq. (5) was solved in the sheath space above the surface. Laplace’s equation was solved within the insulator. Equation (1) was applied at the sheath–insulator interface. The 2D sheath evolved self-consistently under the specified conditions of plasma and insulator properties.

The ion mass and momentum equations were discretized in space using a multidimensional flux-corrected-transport scheme.¹⁴ Time integration was performed using an Adams–Bashforth second-order method. The chosen time step satisfied the Courant–Friderichs–Levy condition. At the end of each time step, Poisson’s equation (Laplace’s equation inside the insulator) was solved to update the electric potential. Integration continued until a periodic steady state was reached.

B. Monte Carlo simulation

The fluid model described above can predict the self-consistent profiles of electric field, ion density, and flux. The *average* energy and angle of ions impinging on the substrate can also be obtained. However, since ions can suffer collisions with the background gas, the fluid model cannot predict the energy and angular *distributions*. MC simulation was used for this purpose.

In the MC simulation, ion trajectories were tracked by integrating the equations of motion

$$\begin{aligned} \frac{\partial v_x}{\partial t} &= \frac{e}{m_i} E_x(x,y,t) \\ \frac{\partial v_y}{\partial t} &= \frac{e}{m_i} E_y(x,y,t) \\ \frac{\partial v_z}{\partial t} &= 0, \end{aligned} \quad (6)$$

where E_x and E_y are the horizontal and vertical components of the electric field, respectively, determined by the fluid simulation; v_x , v_y , and v_z are the components of the ion particle (not fluid) velocity. The spatially nonuniform electric field oscillates at the rf frequency. Ions were launched with the appropriate energy and angular distributions.¹ The

TABLE I. Parameter values used for simulation.

Electron temperature, T_e	3 eV
Electron (ion) density, n_0	$5 \times 10^{10} \text{ cm}^{-3}$
Potential, Φ_0	0 V
Bias voltage, Φ_b	$-50 - 30 \sin(2\pi f_{rf} t)$ V, $f_{rf} = 13.56 \text{ MHz}$
Ar gas pressure	10 mTorr
Gas temperature	0.05 eV
Ion temperature ^a	0.1 eV
Transverse ion temperature ^a	0.1 eV

^aUsed for Monte Carlo simulation only.

launching position was a horizontal plane in the presheath region, away from the (curved) sheath edge. Ions were evenly distributed in space and in the rf phase (0 to 2π).

During their transit through the computational domain, ions can suffer elastic scattering or charge-exchange collisions with background gas. Elastic scattering was treated as a hard sphere collision. For charge-exchange collisions, the fast ion and slow neutral switched identities to become fast neutral and slow ion, respectively, keeping their precollision velocity vector (resonant process). Some 100 000 ions were followed to calculate the ion energy and angular distribution at different locations on the substrate.

IV. RESULTS AND DISCUSSION

The main parameter varied in the simulation was the insulator thickness d , which affected the ratio C_d/C_s . The dielectric constant of the insulator ϵ_r was set at 3.8. Plasma parameters were fixed as shown in Table I. Recall that the origin of the coordinate system is at the insulator-conductor interface (Fig. 4).

The electric potential profile at $t=0.5/f_{rf}$ is shown in Fig. 5(a) for a 150- μm -thick insulator. The potential variation in the sheath ($y>0$) as well as inside the insulator ($-150 \mu\text{m} < y < 0 \mu\text{m}$ and $x < 0 \mu\text{m}$) are shown. Away from the material interface (located at $x=0$), the potential varies only in the vertical direction, reminiscent of a one-dimensional (1D) sheath. The sheath reaches its undisturbed (1D) state over the respective surface far away from the material interface. In the transition region over the material interface, the potential contours gently bend to connect the two sheaths. The sheath potential over the insulator is smaller than the applied bias, because of the voltage drop across the insulator. The sheath potential over the conductor is 50 V, the applied bias voltage at $t=0.5/f_{rf}$, resulting in a thicker sheath.¹⁵ The potential changes abruptly at the sheath-insulator interface (located at $y=0$ and $x<0$). The existence of a surface charge causes a discontinuous jump of E at the interface in accordance with Eq. (1). Far enough to the left-hand side of the material interface, the potential contours are horizontal and equally spaced inside the insulator, i.e., E is $(\Phi_b - \Phi_w)/d$. This linear relation does not hold as the material interface is approached.

The corresponding electric-field vectors (shown for the sheath region only, $y>0$), along with the sheath edge, are plotted in Fig. 5(b). The sheath edge was defined as the locus of points at which the relative net charge density (n_i

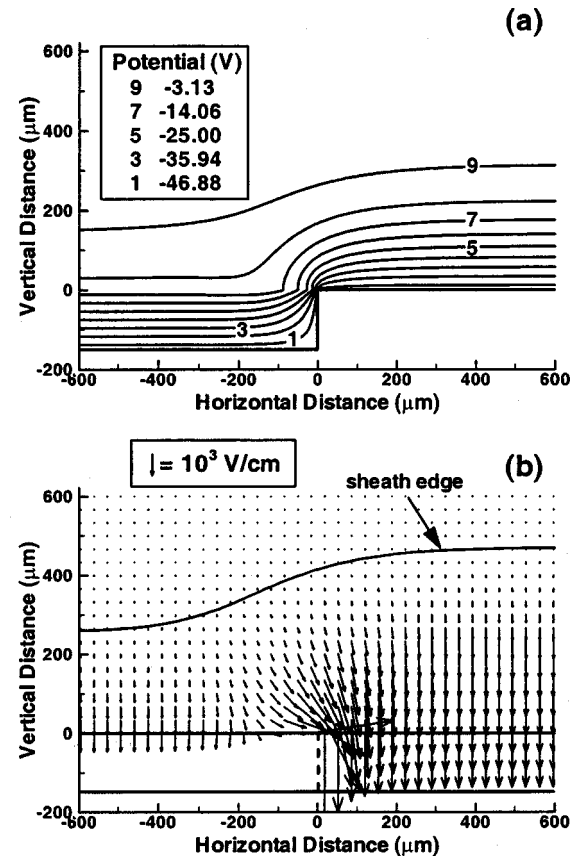


FIG. 5. Electric potential (a) and electric-field vector (b) profiles at $t = 0.5/f_{rf}$ for $d = 150 \mu\text{m}$. Other parameters are shown in Table I. Potential values shown here are referenced with respect to the top boundary, i.e., $\Phi_0 = 0$ V. The electric-field vector is plotted for the sheath region only ($y > 0$). The sheath edge is also shown in (b). The sheath edge was defined as the location where the relative space charge $(n_i - n_e)/n_i$ was 0.01.

$-n_e)/n_i = 0.01$. The electric field is very weak outside the sheath and becomes progressively stronger as the wall is approached. The field is stronger over the conductor, compared to the insulator, due to the larger sheath potential. The field is mainly vertical away from the material interface (1D sheath), but diverges strongly as the interface is neared. Thus, ions will experience quite different trajectories depending on their horizontal location upon entering the sheath.⁶

The IADs at different locations on the substrate are shown in Fig. 6. The top figure in Fig. 6 shows distributions at four different locations on the conductor side; the corresponding distributions on the insulator side are shown in the bottom figure. All distributions were calculated by the MC simulation, using the spatiotemporal electric field found by the fluid simulation. The IAD at $x = 500 \mu\text{m}$ (top figure in Fig. 6) appears to be Gaussian centered at zero degrees, indicating that, away from the interface, ions sample a mainly vertical field (1D sheath). The small angular spread is a result of gas-phase collisions with the background gas experienced in the presheath (ions entering the computational domain have an angular spread). As one approaches the material interface, the electric field possesses a progressively stronger horizontal component [see Fig. 5(b)]. As a result, the IADs on the conductor side shift to larger angles and become broader. The same trends are observed on the insu-

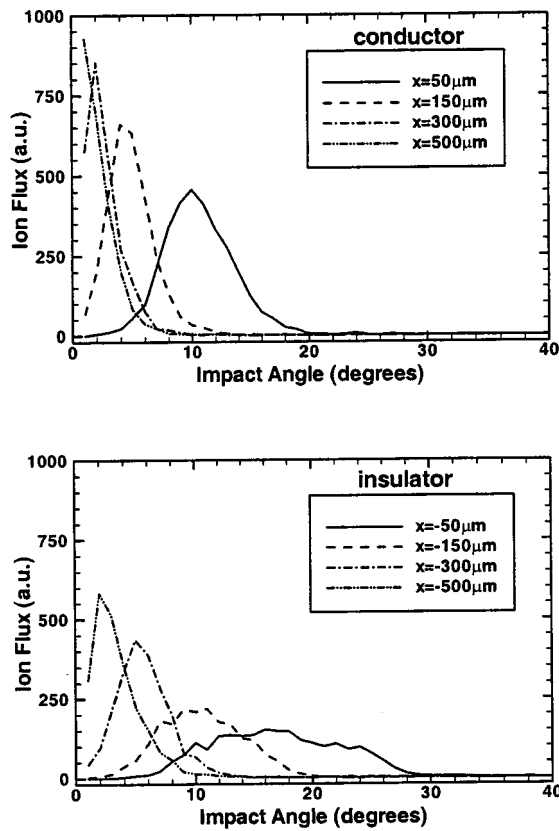


FIG. 6. IADs at different locations on the conductor side (top) and the insulator side (bottom) measured from the interface, for the conditions of Fig. 5.

lator side, but the impact angle and spread of the IAD at the corresponding location are larger. This is because the ion energy over the insulator is smaller (see below) and less energetic ions are easier to deflect. The IAD at $x = -500 \mu\text{m}$ is centered off normal, implying that the sheath has not yet recovered its undisturbed state at that location over the insulator.

The corresponding IEDs are shown in Fig. 7. The double-peaked distributions are nearly identical on the conductor side regardless of the sampling location. The energy spread is ~ 40 V and the high-energy peak is more intense. The IEDs on the conductor are typical for Ar ions in a high-density plasma with a 13.56 MHz sinusoidal bias.¹⁷ For given ion mass, the spread of the IED depends on the sheath thickness and sheath potential wave form.^{16,17} The sheath potential over the conductor is uniform, i.e., $-\Phi_b = 50 + 30 \sin(\omega_{rf}t)$ V, because all applied bias drops across the sheath. Therefore, the IEDs on the conductor side depend solely on the sheath thickness. As the material interface is approached, the sheath over the conductor gets thinner [Fig. 5(b)], resulting in wider IEDs.¹⁷

The IEDs on the insulator side are double peaked as well. However, the IEDs are shifted to lower energies and the low-energy peak is more intense. As one nears the material interface, the energy spread increases, despite the growing sheath thickness. This can be explained by noting that the sheath potential is not uniform along the insulator surface. Figure 8 shows the sheath potential, $\Phi_0 - \Phi_w$ (essentially $-\Phi_w$ since $\Phi_0 = 0$), wave form over the insulator for differ-

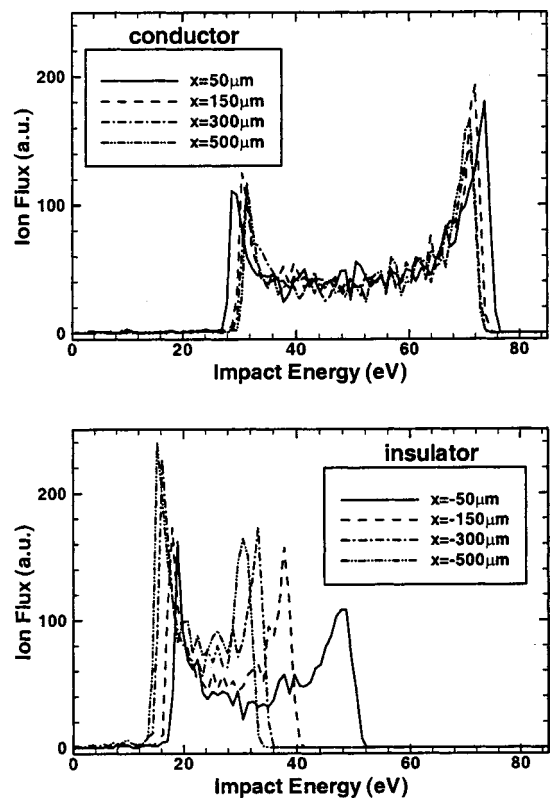


FIG. 7. IEDs at different locations on the conductor side (top) and the insulator side (bottom) measured from the interface, for the conditions of Fig. 5.

ent locations. The applied rf bias wave form (Φ_b) and the corresponding dc floating potential (Φ_{float}) are also shown for comparison. The amplitude of the sheath potential increases as the material interface is approached. In addition, the wave forms are nonsinusoidal, being rather flat near their minimum. Therefore, the resulting IEDs have more intense low-energy peaks. As one moves even closer to the material interface, $\Phi_w(t)$ is progressively approaching $\Phi_b(t)$, indicating that the insulator becomes more strongly coupled to the applied bias, i.e., the ratio C_d/C_s increases. The presence of the vertical equipotential boundary at $x=0$ (where the

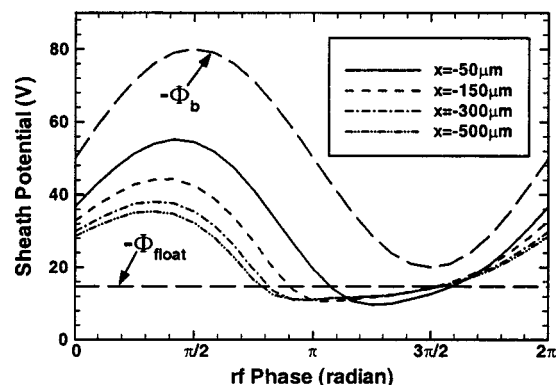


FIG. 8. Sheath potential ($\Phi_0 - \Phi_w$) wave forms at several locations along the insulator surface for the conditions of Fig. 5. The applied bias voltage wave form $\Phi_b(t)$ is also shown. The steady-state floating potential on a flat infinite insulator for a dc condition is $\Phi_{\text{float}} = -14.71$ V.

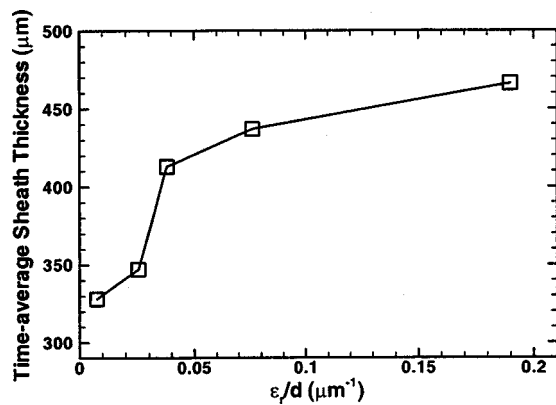


FIG. 9. Time-average thickness of the undisturbed sheath over the insulator at $x = -800 \mu\text{m}$ vs ϵ_r/d . Only d was varied in the simulation, other parameters were set as shown in Table I. Points are simulation predictions, line is for guiding the eye.

insulator on the left-hand side meets the conductor on the right-hand side, see Fig. 4), introduces an “edge” capacitance, increasing the effective C_d .

The time-average sheath thickness over the insulator L_s , calculated at $x = -800 \mu\text{m}$, is plotted versus ϵ_r/d in Fig. 9. Location $x = -800 \mu\text{m}$ is far enough from the material interface for the sheath to recover its 1D state and become planar. The sheath over the insulator grows rapidly with increasing ϵ_r/d and reaches a plateau beyond $\epsilon_r/d \sim 0.1 \mu\text{m}^{-1}$. This occurs as d decreases to the point that the sheath capacitance dominates. The spatial profiles of the time-average insulator surface potential Φ_w are shown for different values of d in Fig. 10. As ϵ_r/d (or C_d/C_s) increases, a smaller potential drop occurs across the insulator. In addition, for given d , as the material interface is approached, the potential drop across the insulator becomes progressively smaller, due to the edge capacitance, as discussed above.

The time-average thickness of the undisturbed sheath over the conductor, calculated at $x = 800 \mu\text{m}$, was $\sim 506 \mu\text{m}$, and was hardly affected by changes in the insulator capacitance, i.e., d . Thus, sheath distortion should be more pronounced and field divergence should be stronger for smaller ϵ_r/d . The time-average ion flux profile along the substrate is plotted for different values of d in Fig. 11. For all cases, the

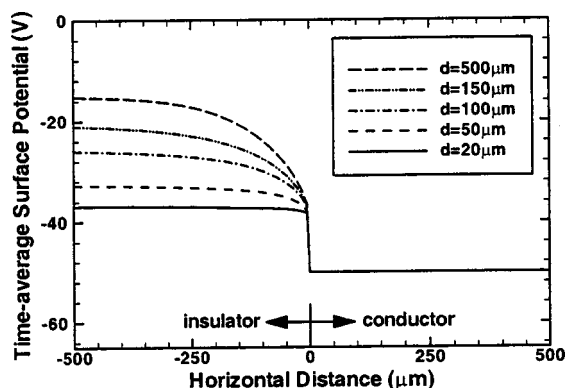


FIG. 10. Time-average surface (wall) potential profile along the substrate as a function of d . The time-average potential of the conductor is -50 V (Table I).

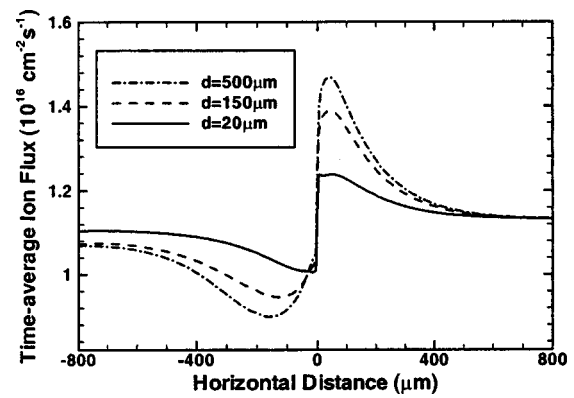


FIG. 11. Time-average ion flux profile along the substrate as a function of d . The undisturbed value of ion flux is always slightly larger on the conductor side because the ion density was assumed spatially uniform along the top boundary of Fig. 4.

ion flux on the conductor side is larger, at the expense of that on the insulator side. This is because the diverging electric field near the material interface (Fig. 5) redirects ions on the conductor side of the interface. As d increases, sheath distortion becomes more pronounced yielding larger differences in the ion flux across the interface. There is a small difference in the ion fluxes over the conductor and the insulator far away from the interface, especially for thicker insulators (when the sheath over the insulator is thinner). This is because the ion density on the upper boundary of the computational domain (Fig. 4) was taken spatially uniform. This can only be satisfied for very large distances from the wall. Thus, the difference in “undisturbed” ion currents is a result of the finite size of the computational domain.

The dependence of rf sheath distortion on ϵ_r/d is also reflected in the ion energy and angular distributions. The average angles and energies, as well as the spreads of the IADs and IEDs are plotted in Figs. 12 and 13, respectively, versus horizontal location along the substrate (recall that $x = 0$ corresponds to the insulator–conductor interface). The trends found in Figs. 6 and 7 are reproduced here: (i) The IADs shift to larger angles and broaden as the material interface is approached from either side of the interface, (ii) ion angular disturbances (in terms of average angle and angular spread) are stronger on the insulator side compared to the conductor side, (iii) the IEDs shift toward larger energies and the energy spread increases as one approaches the material interface from the insulator side, and (iv) the IEDs on the conductor side are rather uniform and the average ion energy is a bit higher than the time-average bias voltage. This is because the input ion energy distribution has a spread of $\sim T_e = 3 \text{ eV}$ and there are hardly any collisions in the thin sheath at 10 mTorr. In addition, there are more ions populating the high-energy peak of the IED, shifting the average to a bit larger values. Furthermore, sheath distortion gets weaker and ion flow becomes more vertical with decreasing d , reducing the ion impact angle and angular spread. Smaller d also favors larger ion impact energy and larger energy spread on the insulator. The IEDs on the conductor are nearly invariant as d changes. The discontinuity in ion properties across the material interface is reduced as d decreases, but remains considerable even for d as low as $20 \mu\text{m}$.

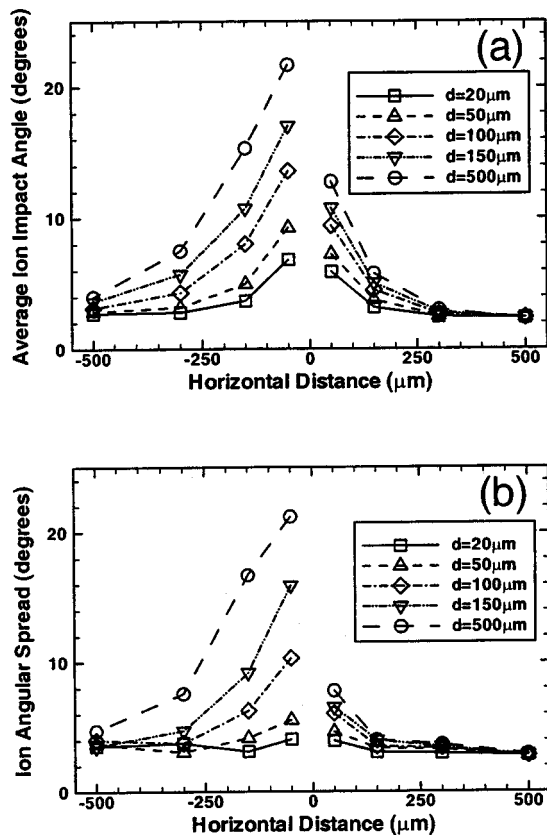


FIG. 12. Average impact angle (a) and angular spread (b) of ions along the substrate. The angular spread was defined as the full width at half-maximum (FWHM) of the IADs. A value of the FWHM was estimated even for non-Gaussian distributions.

V. SUMMARY AND CONCLUSIONS

A combined fluid/MC simulation was employed to study a 2D rf sheath over a flat surface with an insulator-conductor interface in contact with a high-density Ar plasma. The self-consistent fluid simulation predicted the 2D spatiotemporal profiles of the electric field. These were used as input to the MC simulation to predict the IEDs and IADs along the surface.

The capacitance of the insulator increased the local impedance, and made the sheath potential over the insulator smaller than that over the conductor. Thus, for given uniform plasma properties (plasma density and electron temperature), the sheath was thinner over the insulator, compared to that over the conductor. The 2D sheath electric field diverted oncoming ions toward the conductor side of the interface, making the ion flux on the conductor higher at the expense of that on the insulator. The IADs shifted to larger angles off normal, and became broader as the interface was approached from either the conductor or the insulator side of the interface. The IEDs on the insulator side shifted to lower energies and the energy spread decreased as one moved away from the material interface. The IEDs were relatively uniform, reflecting the applied bias, along the conductor side of the interface.

As the insulator thickness d was decreased, the sheath potential over the insulator came closer to that over the conductor, and sheath distortion became less pronounced. Ions

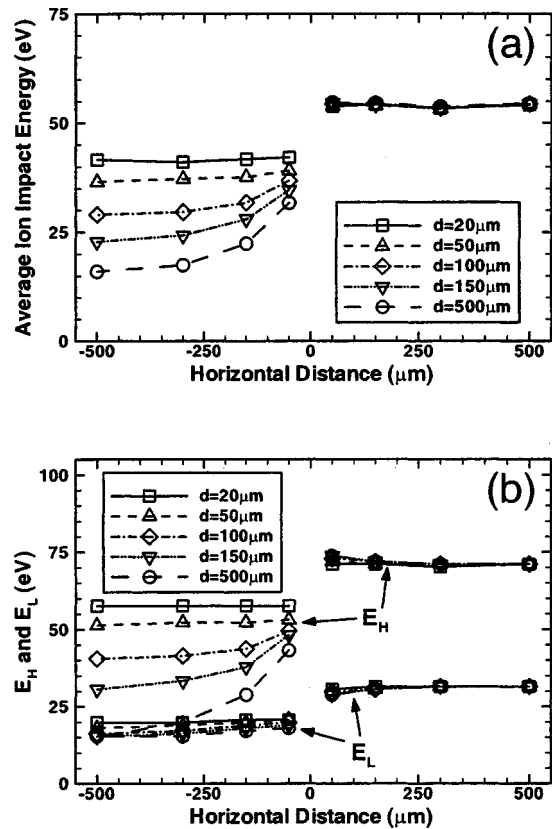


FIG. 13. Average impact energy (a) and energy spread (b) of ions along the substrate. In (b), E_H and E_L represent, respectively, the value of the high-energy peak and the low-energy peak of the double-peaked IEDs. The energy spread was defined as $E_H - E_L$.

experienced less divergence off the vertical for smaller d , and the ion impact angle and angular spread were reduced as d was decreased. Also, the ion impact energy and energy spread on the insulator came closer to their values on the conductor side, as the insulator thickness was reduced. A discontinuity in the ion flux and ion energy and angular distributions across the material interface was still considerable, however, even for d as small as 20 μm .

This work has assumed that the ion density “far away” from the wall is spatially uniform. This may not be the case in practical situations when, for example, the sheath is relatively thick (compared to the mean-free path for ionization) and secondary electron emission from the wall is important. Since the metal portion of the wall may have a different secondary electron emission coefficient than the insulator, ionization in the sheath or modified charging of the insulator, may bring about a spatial profile of the ion density (and even the electron temperature) profile far way from the wall. In addition, when ionization in the sheath is important, the right-hand side of Eq. (3) is no longer zero.

ACKNOWLEDGMENTS

Financial support by the National Institute of Standards and Technology and the National Science Foundation (CTS-0072854) is greatly appreciated. One of the authors (D. K.) is indebted to Professor D. R. Wilton, Electrical and Computer Engineering, University of Houston, for helpful discussions.

Many thanks to Dr. G. Hebner of Sandia National Labs, Albuquerque, NM, for suggesting this problem to the authors.

- ¹D. Kim and D. J. Economou, *IEEE Trans. Plasma Sci.* **30**, 2048 (2002).
²J. R. Woodworth, P. A. Miller, R. J. Shul, I. C. Abraham, B. P. Aragon, T. W. Hamilton, C. G. Willison, D. Kim, and D. J. Economou, *J. Vac. Sci. Technol. A* **21**, 147 (2003).
³D. Kim, D. J. Economou, J. R. Woodworth, P. A. Miller, R. J. Shul, B. P. Aragon, T. W. Hamilton, and C. G. Willison, *IEEE Trans. Plasma Sci.* **31**, 691 (2003); D. Kim and D. J. Economou, *J. Vac. Sci. Technol. B* **21**, 1248 (2003).
⁴D. Kim and D. J. Economou, *J. Appl. Phys.* **94**, 3740 (2003).
⁵C.-K. Kim and D. J. Economou, *J. Appl. Phys.* **91**, 2594 (2002).
⁶D. Kim and D. J. Economou, *J. Appl. Phys.* **94**, 2852 (2003).
⁷R. J. Hoekstra and M. J. Kusher, *J. Appl. Phys.* **77**, 3668 (1995).
⁸A rf electric field can exist in a conductor but it is confined within a thin

region near the surface, the so-called skin depth. If the conductor is perfect (infinite conductivity), the skin depth tends to zero.

- ⁹M. A. Lieberman and A. J. Lichtenberg, *Principles of Plasma Discharges and Materials Processing* (Wiley, New York, 1994).
¹⁰B. Chapman, *Glow Discharge Processes* (Wiley, New York, 1994).
¹¹M. S. Barnes, T. J. Colter, and M. E. Elta, *J. Appl. Phys.* **61**, 81 (1987).
¹²W. H. Hayt, *Engineering Electromagnetics* (McGraw-Hill, New York, 1989).
¹³A. Metzke, D. W. Ernie, and H. J. Oskam, *J. Appl. Phys.* **60**, 3081 (1986).
¹⁴S. T. Zalesak, *J. Comput. Phys.* **31**, 335 (1979).
¹⁵The sheath potential is usually defined as the difference in the potential between the sheath edge and the substrate surface. However, since the potential drop outside the sheath is very small, the sheath potential is approximately equal to the difference in potential between the top boundary (Fig. 4) and the surface ($\Phi_0 - \Phi_w$).
¹⁶M. A. Sobolewski, Y. Wang, and A. Goyette, *J. Appl. Phys.* **91**, 6303 (2002).
¹⁷T. Panagopoulos and D. J. Economou, *J. Appl. Phys.* **85**, 3435 (1999).